The Journal of Chemical Physics

RAPID COMMUNICATION | APRIL 24 2023

Computing chemical potentials of adsorbed or confined fluids

Rochus Schmid ; Bingqing Cheng

J. Chem. Phys. 158, 161101 (2023)
https://doi.org/10.1063/5.0146711

AIP Publishing

The Journal of Chemical Physics COMMUNICATION scitation.org/journal/jcp

Computing chemical potentials of adsorbed or confined fluids

Cite as: J. Chem. Phys. 158, 161101 (2023); doi: 10.1063/5.0146711
Submitted: 16 February 2023 • Accepted: 3 April 2023 •
Published Online: 24 April 2023

Rochus Schmid[1] and Bingqing Cheng[2,a)]

AFFILIATIONS

[1] Computational Materials Chemistry Group, Faculty of Chemistry and Biochemistry, Ruhr-Universität Bochum, Universitätsstr. 150, 44801 Bochum, Germany
[2] The Institute of Science and Technology Austria, Am Campus 1, 3400 Klosterneuburg, Austria

[a)] **Author to whom correspondence should be addressed:** bingqing.cheng@ist.ac.at

ABSTRACT

The chemical potential of adsorbed or confined fluids provides insight into their unique thermodynamic properties and determines adsorption isotherms. However, it is often difficult to compute this quantity from atomistic simulations using existing statistical mechanical methods. We introduce a computational framework that utilizes static structure factors, thermodynamic integration, and free energy perturbation for calculating the absolute chemical potential of fluids. For demonstration, we apply the method to compute the adsorption isotherms of carbon dioxide in a metal-organic framework and water in carbon nanotubes.

I. INTRODUCTION

Confinement in a small volume, such as inside a nanotube or an ion channel, or adsorption to a porous material can significantly change the chemical potential of a fluid.[1] The chemical potential directly determines the adsorption isotherm, which is the relationship between the amount of a gas or liquid that is adsorbed and the pressure or concentration of the gas or liquid in the surrounding reservoir. This relationship is important for porous materials because it determines their capacity to store and separate fluids[1] and can also have a significant impact on their physical and chemical properties.[2] The adsorption isotherm also helps understand the phase behavior[3,4] and the transport phenomena of confined fluids.[5]

Computing chemical potentials from atomistic simulations can be challenging, especially for confined or adsorbed fluids. Many methods[6–14] have caveats and only work for a subset of systems: Monte Carlo particle insertion and removal[15,16] can have problems with low insertion probability or numerical convergence issues.[10] Thermodynamic integration (TI) or the overlapping distribution method[6,7] may have singularity problems at the end points of the integration.[12,13] Moreover, pressure, which enters the TI expression along an isotherm, is ill-defined for confined systems[17,18] or heterogeneous fluids.[19]

The recent S0 method[20] brings a new perspective for the chemical potentials of mixtures. This method utilizes the thermodynamic relationship between the particle number fluctuations and the derivatives of the chemical potentials with respect to the molar concentration and only uses the static structure factors computed from equilibrium molecular dynamics (MD) simulations at different mixture fractions. However, there are a couple of leaps to be made to apply the method to the chemical potentials of adsorbed or confined fluids. First, the S0 method evaluates the relative chemical potential as a function of concentration c for each phase, and one needs to establish the relation between these relative values of different phases. Second, the method was developed for fluid mixtures, so one needs to extend it to other situations.

Here, we introduce a statistical mechanical method [S0—thermodynamic integration and free energy perturbation (TIFEP)] to compute the chemical potentials and the adsorption isotherms of adsorbed or confined fluids. We then benchmark the applicability of the method for the simple system of an argon fluid in a metal-organic framework (MOF), a carbon dioxide fluid in MOF-5, an archetypical rigid metal organic framework with a

cubic pore structure,[21] and water in single-walled carbon nanotubes (CNTs).

II. THEORY

The general workflow is illustrated in Fig. 1. For the adsorbed phase, one first computes the absolute chemical potential at a certain low loading using a combination of thermodynamic integration and free energy perturbation (TIFEP) and then determines the chemical potentials at other concentrations using the S0 method. For the pure phase, the same approach applies, although sometimes one can compute $\mu(c)$ directly starting from the dilute limit using the S0 method or TI. In what follows, we describe each step of the workflow.

A. Absolute chemical potential

The absolute chemical potential, μ, at a certain particle concentration, c, can be split into an ideal and an excess part,

$$\mu = \mu^{id}(c) + \mu^{ex}, \tag{1}$$

where the ideal part can be analytically expressed as $\mu^{id}(c) = \mu_0 + k_B T \ln(c/c_0)$. The excess part, μ^{ex}, is the Gibbs free energy difference between a particle that is fully-interacting with its surroundings and the same particle in the ideal-gas state. To evaluate μ^{ex}, the conventional method is to use Widom particle insertion, but in the supplementary material, we show that the TIFEP approach (the purple and blue arrows in Fig. 1) is more robust and statistically efficient. The TI is performed along a reversible path between the physical system and a reference system over a switching parameter λ.[22,23] Other procedures for the Hamiltonian switching are available, and some may help with numerical stability,[24,25] but here we adopt linear λ scaling for simplicity. The parameterized Hamiltonian is

$$\mathcal{H}(\lambda) = (1-\lambda)\mathcal{H}_{no-inter} + \lambda\mathcal{H}, \tag{2}$$

where $\mathcal{H}$ is the actual Hamiltonian, and $\mathcal{H}_{no-inter}$ is for the reference system with no interaction between one ghost molecule and the rest of the system. In $\mathcal{H}_{no-inter}$, the intramolecular energy and forces of the ghost molecule and all the interactions between the rest of the system stay the same as in $\mathcal{H}$. The excess free energy of the extra molecule can then be evaluated using

$$\mu^{ex} = \int_0^1 d\lambda \langle U - U_{no-inter}\rangle_\lambda, \tag{3}$$

where $\langle\cdots\rangle_\lambda$ denotes the ensemble average using the Hamiltonian $\mathcal{H}(\lambda)$ in the canonical ensemble (NVT) or isothermal-isobaric ensemble (NPT) simulations. However, the integrand in Eq. (3) is divergent at $\lambda = 0$ because when the ghost molecule and the rest of the system are not interacting at all, the atoms can overlap and cause extremely large energy differences $U - U_{no-inter}$. This problematic bit is indicated by the blue dashed arrow in Fig. 1. To circumvent this issue, one can perform a free energy perturbation (FEP) at the end point (purple arrow in Fig. 1), i.e.,

$$\Delta\mu_\epsilon^{ex} = -k_B T \ln\left\langle \exp\left[-\frac{\epsilon(U - U_{no-inter})}{k_B T}\right]\right\rangle_{\lambda=0}, \tag{4}$$

where ϵ is a small number, which we typically set to about 0.05, though it can be flexible. Such an FEP procedure can also be used for other segments of the switching besides the end point, i.e., $\mu_{\lambda+\epsilon}^{ex} - \mu_\lambda^{ex}$, in order to eliminate the numerical error in the TI.[23,25] In principle, one can also evaluate $\Delta\mu_\epsilon^{ex}$ with $H(\epsilon)$ using a backward FEP, but this is less statistically efficient because in the exponential average of the backward FEP, low-occurrence outliers will yield extremely large contributions.[25,26] The excess chemical potential is thus

$$\mu^{ex} = \Delta\mu_\epsilon^{ex} + \int_\epsilon^1 d\lambda \langle U - U_{no-inter}\rangle_\lambda. \tag{5}$$

B. Concentration-dependent μ

One can use the S0 method to compute the concentration dependency in μ, as schematically shown by the black arrow in Fig. 1. To extend the S0 method in Ref. 20 to a fluid that is adsorbed or confined in a porous medium that is without frozen long-range disorder, there are two views: The first view is to regard the fluid and

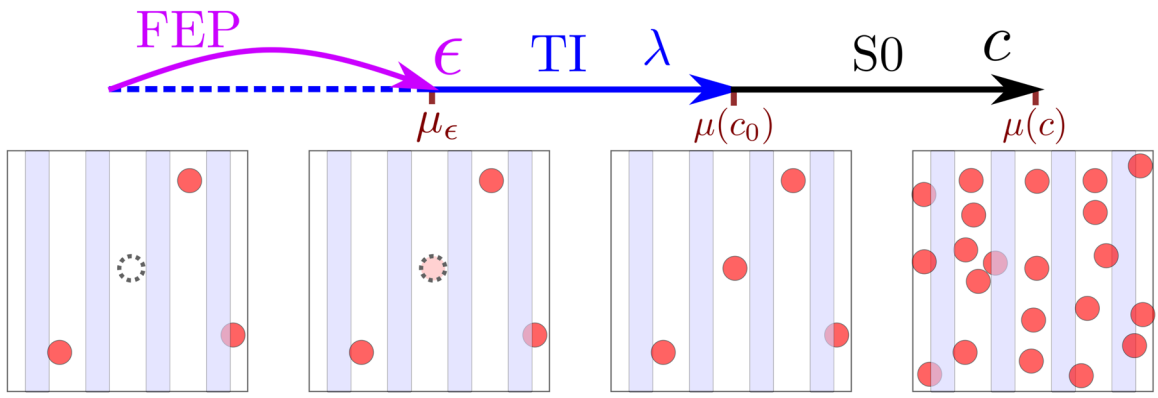

FIG. 1. The thermodynamic framework for computing the absolute chemical potential of adsorbed or confined fluid. The TIFEP method for calculating the excess chemical potential at concentration c_0 is shown by the purple and blue arrows: first, use FEP to add ϵ fraction of a molecule, and then reversibly switch this fraction of a molecule to a fully-interacting one in TI. The black arrow indicates using the S0 method to compute the chemical potential at different concentrations c.

the medium as two components, and the latter component is an immobile single molecule with zero associated density fluctuations. The second view is to only analyze the density fluctuations of the fluid while treating the medium as a background that only provides an external potential energy field. The two views result in the same thermodynamic relations, and here we focus on the second one and introduce the single-component formulation of the S0 method.

For a single-component system or a single-component system adsorbed in a homogeneous material without arrested defects (e.g., crystallographic defects), the particle number fluctuations in the grand-canonical ensemble (constant-μVT) are related to the chemical potential by[27]

$$\frac{\langle (N-\langle N\rangle)^2\rangle_{\mu VT}}{\langle N\rangle_{\mu VT}} = \frac{k_B T}{\langle N\rangle_{\mu VT}}\left(\frac{\partial\langle N\rangle}{\partial\mu}\right)_{V,T}. \tag{6}$$

The structure factor is related to the particle number fluctuations via[20]

$$S^0 \equiv \lim_{\mathbf{k}\to 0} S(\mathbf{k}) = \frac{\langle (N-\langle N\rangle)^2\rangle_{\mu VT}}{\langle N\rangle_{\mu VT}}, \tag{7}$$

where

$$S(\mathbf{k}) = \frac{1}{N}\langle \tilde{\rho}(\mathbf{k},t)\tilde{\rho}(-\mathbf{k},t)\rangle, \tag{8}$$

with

$$\tilde{\rho}(\mathbf{k},t) = \int_V d\mathbf{r}\rho(\mathbf{r},t)\exp(i\mathbf{k}\cdot\mathbf{r}) = \sum_{i=1}^{N}\exp(i\mathbf{k}\cdot\mathbf{r}_i(t)). \tag{9}$$

In practice, one can compute $S(\mathbf{k})$ at small $\mathbf{k}$ from NVT or NPT MD simulations and extrapolate to the $\mathbf{k}\to 0$ case to get S^0, as detailed in Ref. 20.

Taking the molar concentration as $c = N/V = \langle N\rangle_{\mu VT}/V$ and combining Eq. (6) with Eq. (7), we obtain

$$\left(\frac{\partial\mu}{\partial c}\right)_T = \frac{k_B T}{cS^0}. \tag{10}$$

Importantly, Eq. (10) works across phase transitions and the coexistence region for large systems; if the overall c of the system is between the molar concentrations of two coexisting phases, both phases will appear simultaneously with macroscopic phase boundaries, which will cause S^0 to diverge so $\frac{\partial\mu}{\partial c}$ under coexistence will be correctly predicted to vanish.

As the key equation of the method, one can obtain $\mu(c)$ using numerical integration with respect to c,

$$\mu(c) = \mu(c_0) + k_B T\ln\left(\frac{c}{c^0}\right) + k_B T\int_{\ln c^0}^{\ln c} d\ln(c)\left[\frac{1}{S^0}-1\right]. \tag{11}$$

Notice that a change of the variable $y = \ln(c)$ is performed to reduce the numerical errors in the integration.

Equations (5) and (11) can then be combined to obtain the chemical potentials of the adsorbed or pure fluids. Moreover, for a pure fluid, $d\mu = (1/c)dP$ along the isotherm, S^0 thus determines the pressure via

$$\left(\frac{\partial P}{\partial c}\right)_T = \frac{k_B T}{S^0}, \tag{12}$$

which becomes the ideal gas law $P = ck_B T$ when $S^0 = 1$. Equation (12) can be useful when the equation of state (EOS) is difficult to compute directly. Furthermore, from $\frac{\partial\mu}{\partial c}\frac{\partial c}{\partial P}$, it is easy to verify that

$$\left(\frac{\partial\mu}{\partial P}\right)_T = \frac{1}{c}, \tag{13}$$

which is a useful relationship for computing the μ of pure liquids using thermodynamic integration along the isotherm. However, unlike the S0 route, Eq. (13) is not applicable to systems with ill-defined pressures or across phase transitions.

III. RESULTS

We first validate our method on argon adsorption in MOF-5 at 370 K since a number of free energy methods, such as TI, FEP, and coexistence simulations, work for this monoatomic gas at high T and allow a benchmark. Indeed, as detailed in the supplementary material, all methods, including S0-TIFEP, give consistent results. We then showcase our method on the two systems shown in Fig. 2: carbon dioxide in MOF-5 and water in single-walled CNTs.

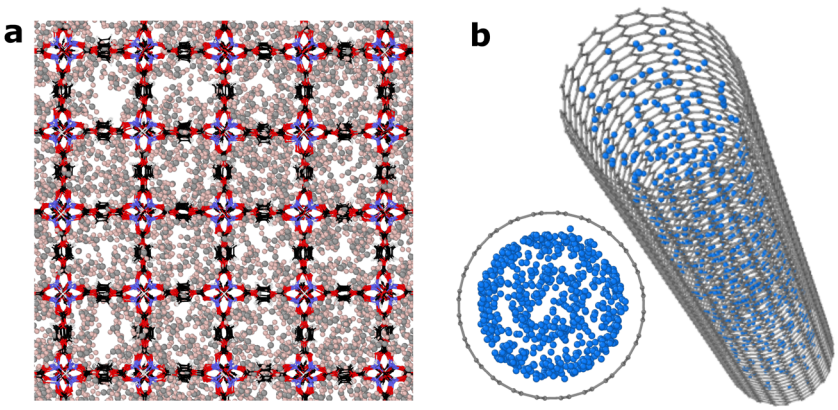

FIG. 2. Systems of study. Carbon dioxide in MOF-5 (a) and water in a single-walled CNT (b).

A. Carbon dioxide in MOF-5

The archetypical MOF-5 (or IRMOF-1)[21] is formed by a Zn_4O inorganic building unit connected by the ditopic terephthalate linker in an octahedral fashion. Its interaction with gas has been intensively studied both experimentally and theoretically,[28–32] particularly for the adsorption of carbon dioxide (CO_2).[33]

We simulated CO_2 in MOF-5 and gas-phase CO_2 at 218 and 300 K using the fully flexible, first-principles-derived force field MOF-FF.[34,35] Details on the force field parametrization and benchmarks can be found in the supplementary material. We first computed the excess chemical potential μ^{ex} for infinitely-diluted CO_2 in MOF-5 using the TIFEP method by switching from a fully-interacting MOF-5 and one CO_2 molecule system to a reference state that has the MOF-5 and a non-interacting ghost CO_2 molecule, using a $1 \times 1 \times 1$ MOF-5 cell. We ran independent simulations on a dense grid of λ, with $\epsilon = 0.01$. Crucially, a combination of a stochastic velocity rescaling thermostat[36] and a weak local Langevin thermostat was used to ensure sufficient equilibration of the ghost molecule.

We then computed the concentration dependence of the chemical potentials for CO_2 in MOF-5 as well as for gas-phase CO_2 using the S0 method. We performed LAMMPS[37] NPT simulations at 1 bar for a $6 \times 6 \times 6$ supercell of MOF-5 loaded with different amounts of CO_2 and NVT simulations of the pure carbon dioxide gas with a similar cell size at a range of c. We used a timestep of 1 fs since the resulting S0 is consistent with the ones at a smaller time step of 0.1 fs. From the MD trajectories, we calculated $S(\mathbf{k})$ from Eqs. (8) and (9) and extracted S^0, as detailed in the supplementary material.

To determine the EOS for the gas CO_2, we used Eq. (12) employing S0, which is efficient and insensitive to the timestep, as shown in Fig. 3(a). Alternatively, one can take the average P in the NVT simulations, but for CO_2, this has caveats: the intramolecular bonds are quite stiff, and a tiny time step is needed to properly integrate the equation of motion because the coupling between the van der Waals interactions and the bonds is so weak that it is difficult to equilibrate the latter properly. One thus has to use a small timestep of 0.1 fs and again use a combination of a stochastic velocity rescaling thermostat[36] and a weak local Langevin thermostat. Overall, the EOS of gas CO_2 at low concentrations is rather close to the ideal gas state.

The chemical potentials for the pure and the adsorbed carbon dioxide are plotted in Fig. 3(b). For the pure gas, the S0 results (blue dashed curve) agree well with the TI along the isotherm [Eq. (13)]. For CO_2 in MOF-5, we performed additional independent TIFEP calculations at higher concentrations (hollow symbols), which agree well with the values obtained using S0 together with TIFEP at the dilute concentration (red dashed curves).

To compute the absolute adsorption isotherm, one relates the concentrations of bulk and adsorbed carbon dioxide that correspond to the same absolute μ and plots the adsorbed concentration against the pressure of the bulk phase. In Fig. 3(c), the equilibrium concentrations of CO_2 adsorbed in MOF-5 at 218 and 300 K are plotted as a function of the pressure of the gas reservoir. MOF-5 can adsorb a large amount of carbon dioxide.

As the pressure increases, the material becomes saturated, and the capability of carbon dioxide adsorption decreases. For both temperatures, we observe an inflection and a type V isotherm, which

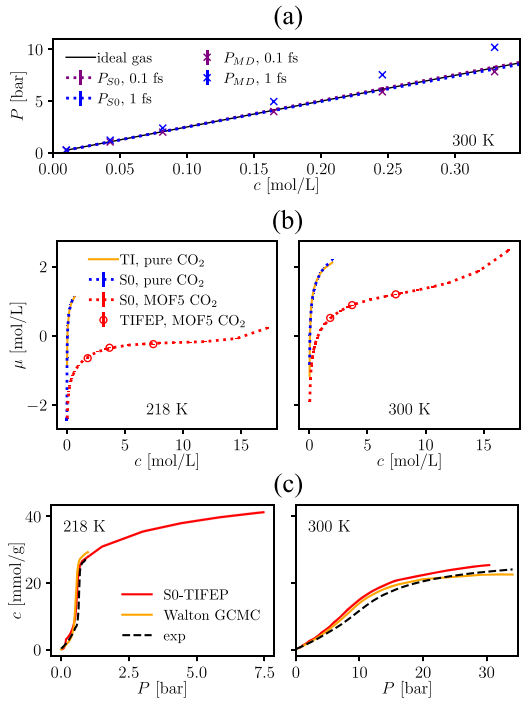

FIG. 3. (a): The equation of state for gas carbon dioxide. (b): The chemical potentials of carbon dioxide molecules in the gas phase and adsorbed in the MOF-5, computed using different TIFEPs directly (hollow symbols) and using S0 together with TIFEP at a low concentration (dashed curves). Error bars are smaller than the symbols. (c): The absolute adsorption isotherm for carbon dioxide in MOF-5. The shaded red areas indicate the uncertainty in our S0-TIFEP calculations, but they are too narrow to be seen. Experimental and GCMC results from Ref. 33 are shown for comparison.

are more pronounced at the lower temperature. The same type V was observed previously experimentally and in grand canonical Monte Carlo (GCMC) simulations.[33] A type V isotherm is usually considered to be quite rare in microporous adsorption. Our simulated isotherms well-capture the overall shape of the experimental curves at both temperatures, although the simulated curve at 300 K is slightly higher, which may be attributed to the defect-free MOF-5 in simulations or the force field assumed. Differences between our results and the previous GCMC isotherms[33] may be due to the different force fields since they used a rigid MOF-5 with the TraPPE potential for CO_2.[38]

B. Water in CNTs

Carbon nanotubes have unique physical and chemical properties, in particular their capacity to store or convey water.[39] We performed simulations for (8:8) and (12:12) single-walled CNTs and water using a simple mW model[40] at 273 and 500 K, with the same parameterization as the graphitic and water systems in Ref. 41. Note that the force fields for CNT-water are a controversial topic,[39,42] and we do not intend to provide a definitive picture for this complex system but only to demonstrate our methodology.

The TIFEP part was computed from small systems, and the S0 was performed on large systems, as described in the supplementary material. For water in the CNT, S^0 was evaluated from $S(\mathbf{k})$ with $\mathbf{k}$ parallel to the direction of the CNT. Here, the c was defined by the total number of water molecules and the entire volume enclosed by the radius of the CNT. One can define c differently to consider the volume occupied by the carbon atoms at the wall, but this will only introduce a constant scaling factor, αc, with α close to 1. Equation (10) indicates that the scaling α does not affect the values of μ.

For pure water with ρ less than about 1 g/ml, CNT (12:12)-water with ρ less than about 0.6 g/ml, and CNT (8:8)-water with ρ less than about 0.6 g/ml, the systems show liquid–vapor coexistence. At these conditions, the presence of the interfaces has an influence on the pressure via the Laplace equation,[19] making the actual pressure difficult to compute. Moreover, pressure is not well-defined for nanoconfined fluids as sizes and stress tensors along the small dimensions are ambiguous.[17,18] These make it problematic to obtain μ using TI along isotherms [Eq. (13)]. In contrast, the S0 method has no problem handling coexistence: S^0 approaches infinity, giving zero $\frac{\partial P}{\partial c}$ and zero $\frac{\partial \mu}{\partial c}$ for coexistence systems. The nanoconfinement is taken into account by only analyzing S^0 along the unconfined dimension.

The chemical potentials for bulk and confined water are plotted in Fig. 4(a). The values obtained using S0 together with TIFEP at a low concentration (dashed curves) agree well with independent TIFEP at higher concentrations (hollow symbols). For systems in the liquid–vapor coexistence region, μ is constant, showing the capability of the S0 method to cross phase boundaries. At low concentrations, bulk water has a lower μ than confined water, but confined water has a slower chemical potential increase and becomes more thermodynamically favorable at higher densities. Bulk water exhibits a solid–liquid phase transition at about 1.2 g/ml at 273 K and 1.5 g/ml at 500 K in the MD simulations, while such transitions are absent in the CNT-water.

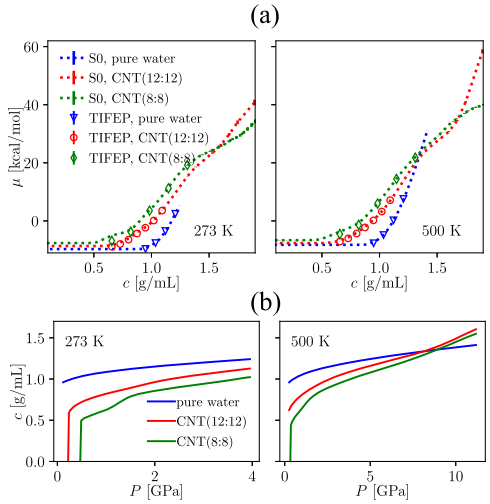

FIG. 4. (a): Chemical potentials of pure water and water in CNTs computed using different methods. Error bars are smaller than the symbols or the linewidth. (b): The adsorption isotherm for water.

The adsorption isotherm is shown in Fig. 4(b), with the pressure of the bulk water plotted on the x axis. Note that the absorption isotherm here is based on the thermodynamic equilibrium argument, which avoids the adsorption–desorption hysteresis loops in the direct simulations.[43] CNT (8:8) has little water adsorption at zero pressure, followed by a steep increase in water intake around 0.5 GPa at both 273 and 500 K. Such adsorption behavior exhibits the typical features of type V adsorption isotherms and is in agreement with previous simulation results.[43] CNT (12:12) follows a similar trend at 273 K, but with a lower threshold pressure of 0.25 GPa. At a high P of more than 10 GPa, the CNT (8:8) is most efficient in adsorbing water.

IV. CONCLUSIONS

Here, we introduce a thermodynamic framework that computes the absolute chemical potentials of confined or adsorbed fluids and determines the pressure in an efficient way. Compared to the conventional FEP and GCMC at a fixed concentration or chemical potential, the possibility to calculate the concentration dependence of μ using the S0 method allows robust computation of μ for dense systems, although larger system sizes are required in simulations. Moreover, the S0-TIFEP method only relies on standard MD software and naturally incorporates the flexibility of adsorbed molecules and porous materials. We envisage this method being applied to many technologically important systems for which the chemical potentials of confined or adsorbed fluids can be useful; understanding the thermodynamics is key to exploring the exotic phases of matter under confinement;[3,4] the chemical potentials of molecules adsorbed in porous materials are crucial for the performance of fuel cells,[44] gas storage and separation,[1] the reactivity of fluids adsorbed in porous catalysts,[45] oil recovery systems,[46] and environmental pollution management.[47]

SUPPLEMENTARY MATERIAL

The supplementary material contains additional information about the molecular dynamics simulations and analysis.

ACKNOWLEDGMENTS

We thank Aleks Reinhardt and Daan Frenkel for their insightful comments and suggestions on the article. B.C. acknowledges the resources provided by the Cambridge Tier-2 system operated by the University of Cambridge Research Computing Service funded by EPSRC Tier-2 capital Grant No. EP/P020259/1.

AUTHOR DECLARATIONS

Conflict of Interest

The authors have no conflicts to disclose.

Author Contributions

Rochus Schmid: Conceptualization (equal); Methodology (supporting); Writing – original draft (supporting); Writing – review & editing (equal). **Bingqing Cheng**: Conceptualization (equal); Methodology (lead); Writing – original draft (lead); Writing – review & editing (equal).

DATA AVAILABILITY

Additional simulation details are provided in the supplementary material. All Python scripts and simulation input files generated for the study are in the supplementary material repository at https://github.com/BingqingCheng/mu-adsorption. Scripts for the S0 analysis are at https://github.com/BingqingCheng/S0.

REFERENCES

[1] L. D. Gelb, K. E. Gubbins, R. Radhakrishnan, and M. Sliwinska-Bartkowiak, Rep. Prog. Phys. **62**, 1573 (1999).
[2] L. Fumagalli, A. Esfandiar, R. Fabregas, S. Hu, P. Ares, A. Janardanan, Q. Yang, B. Radha, T. Taniguchi, K. Watanabe *et al.*, Science **360**, 1339 (2018).
[3] V. Kapil, C. Schran, A. Zen, J. Chen, C. J. Pickard, and A. Michaelides, Nature **609**, 512 (2022).
[4] G. Algara-Siller, O. Lehtinen, F. C. Wang, R. R. Nair, U. Kaiser, H. A. Wu, A. K. Geim, and I. V. Grigorieva, Nature **519**, 443 (2015).
[5] N. Kavokine, M.-L. Bocquet, and L. Bocquet, Nature **602**, 84 (2022).
[6] E. Sanz and C. Vega, J. Chem. Phys. **126**, 014507 (2007).
[7] A. S. Paluch, S. Jayaraman, J. K. Shah, and E. J. Maginn, J. Chem. Phys. **133**, 124504 (2010).
[8] M. Lísal, W. R. Smith, and J. Kolafa, J. Phys. Chem. B **109**, 12956 (2005).
[9] F. Moučka, M. Lísal, J. Škvor, J. Jirsák, I. Nezbeda, and W. R. Smith, J. Phys. Chem. B **115**, 7849 (2011).
[10] C. Perego, F. Giberti, and M. Parrinello, Eur. Phys. J. Spec. Top. **225**, 1621 (2016).
[11] I. S. Joung and T. E. Cheatham III, J. Phys. Chem. B **112**, 9020 (2008).
[12] L. Li, T. Totton, and D. Frenkel, J. Chem. Phys. **146**, 214110(2017).
[13] L. Li, T. Totton, and D. Frenkel, J. Chem. Phys. **149**, 054102 (2018).
[14] H. A. Vinutha and D. Frenkel, J. Chem. Phys. **154**, 124502 (2021).
[15] M. P. Allen and D. J. Tildesley, *Computer Simulation in Chemical Physics* (Springer Science and Business Media, 2012), Vol. 397, pp. 108–111.
[16] B. Smit and D. Frenkel, Mol. Phys. **68**, 951 (1989).
[17] F. Varnik, J. Baschnagel, and K. Binder, J. Chem. Phys. **113**, 4444 (2000).
[18] K. Shi, E. R. Smith, E. E. Santiso, and K. E. Gubbins, J. Chem. Phys. **158**, 040901 (2023).
[19] S. Marchio, S. Meloni, A. Giacomello, C. Valeriani, and C. M. Casciola, J. Chem. Phys. **148**, 064706 (2018).
[20] B. Cheng, J. Chem. Phys. **157**, 121101 (2022).
[21] H. Li, M. Eddaoudi, M. O'Keeffe, and O. M. Yaghi, Nature **402**, 276 (1999).
[22] D. Frenkel and A. J. C. Ladd, J. Chem. Phys. **81**, 3188 (1984).
[23] B. Cheng and M. Ceriotti, Phys. Rev. B **97**, 054102(2018).
[24] T. C. Beutler, A. E. Mark, R. C. van Schaik, P. R. Gerber, and W. F. van Gunsteren, Chem. Phys. Lett. **222**, 529 (1994).
[25] N. Lu and D. A. Kofke, J. Chem. Phys. **114**, 7303 (2001).
[26] B. Cheng and M. Ceriotti, J. Phys. Chem. B **141**, 244112 (2014).
[27] J. G. Kirkwood and F. P. Buff, J. Chem. Phys. **19**, 774 (1951).
[28] J.-R. Li, R. J. Kuppler, and H.-C. Zhou, Chem. Soc. Rev. **38**, 1477 (2009).
[29] R. B. Getman, Y.-S. Bae, C. E. Wilmer, and R. Q. Snurr, Chem. Rev. **112**, 703 (2012).
[30] H. Furukawa, K. E. Cordova, M. O'Keeffe, and O. M. Yaghi, Science **341**, 1230444 (2013).
[31] H.-C. Zhou, J. R. Long, and O. M. Yaghi, "Introduction to metal–organic frameworks," Chem. Rev. **112**, 673 (2012).
[32] K. Sumida, D. L. Rogow, J. A. Mason, T. M. McDonald, E. D. Bloch, Z. R. Herm, T.-H. Bae, and J. R. Long, Chem. Rev. **112**, 724 (2012).
[33] K. S. Walton, A. R. Millward, D. Dubbeldam, H. Frost, J. J. Low, O. M. Yaghi, and R. Q. Snurr, J. Am. Chem. Soc. **130**, 406 (2007).
[34] S. Bureekaew, S. Amirjalayer, M. Tafipolsky, C. Spickermann, T. K. Roy, and R. Schmid, Phys. Status Solidi B **250**, 1128 (2013).
[35] J. Keupp, J. P. Dürholt, and R. Schmid, Faraday Discuss. **225**, 324 (2021).
[36] G. Bussi, D. Donadio, and M. Parrinello, J. Chem. Phys. **126**, 014101 (2007).
[37] S. Plimpton, J. Comput. Phys. **117**, 1 (1995).
[38] J. J. Potoff and J. I. Siepmann, AIChE J. **47**, 1676 (2001).
[39] A. Alexiadis and S. Kassinos, Chem. Rev. **108**, 5014 (2008).
[40] V. Molinero and E. B. Moore, J. Phys. Chem. B **113**, 4008 (2009).
[41] M. B. Davies, M. Fitzner, and A. Michaelides, Proc. Natl. Acad. Sci. U. S. A. **118**, e2025245118 (2021).
[42] T. Werder, J. H. Walther, R. L. Jaffe, T. Halicioglu, and P. Koumoutsakos, J. Phys. Chem. B **107**, 1345 (2003).
[43] A. Striolo, A. A. Chialvo, K. E. Gubbins, and P. T. Cummings, J. Chem. Phys. **122**, 234712 (2005).
[44] H. Wang, X. Wang, M. Li, L. Zheng, D. Guan, X. Huang, J. Xu, and J. Yu, Adv. Mater. **32**, 2002559 (2020).
[45] A. G. Slater and A. I. Cooper, Science **348**, aaa8075 (2015).
[46] M. O. Adebajo, R. L. Frost, J. T. Kloprogge, O. Carmody, and S. Kokot, J. Porous Mater. **10**, 159 (2003).
[47] X. Liu, G. Verma, Z. Chen, B. Hu, Q. Huang, H. Yang, S. Ma, and X. Wang, Innovation **3**, 100281 (2022).